arXiv:2205.06148v1 [physics.optics] 12 May 2022

Spatially resolved spectroscopy of alkali metal vapour diffusing inside hollow-core photonic crystal fibres

Daniel R Häupl[1,2], Daniel Weller[3], Robert Löw[3] and Nicolas Y Joly[1,2]

[1] University of Erlangen-Nürnberg, Staudtstraße 7/B2, 91058 Erlangen, Germany
[2] Max Planck Institute for the Science of Light, Staudtstraße 2, 91058 Erlangen, Germany
[3] 5th Physical Institute, University of Stuttgart, Pfaffenwaldring 57, 70569 Stuttgart, Germany

E-mail: daniel.haeupl@mpl.mpg.de

Abstract. We present a new type of compact and all-glass based vapour cell integrating hollow-core photonic crystal fibres. The absence of metals, as in a traditional vacuum chamber and the much more compact geometry allows for fast and homogeneous heating. As a consequence we can fill the fibres on much faster timescales, ranging from minutes to hours. Additionally the all-glass design ensures optical access along the fibre. This allows live monitoring of the diffusion of rubidium atoms inside the hollow-core by measuring the frequency-dependent fluorescence from the atoms. The atomic density is numerically retrieved using a 5-level system of Bloch-equations.

1. Introduction

Hot atomic vapours are an active field of research and have great potential in the fields of quantum optics [1, 2] quantum communication [3, 4] or metrology [5, 6]. Optimal atom-light coupling in a vapour cell is limited by the diffraction limit of Gaussian beams. This can be overcome by confining light and atoms inside a hollow-core fibre. This led to many applications from nonlinear optics in noble gases [7], to chemistry [8], and three-photons spectroscopy of caesium vapour inside PCFs [9]. Although previous works [9–11] showed the feasibility of filling HC-PCFs with hot vapours, the experimental setup was not optimal. The fibres were placed inside a conventional steel vacuum chamber filled with caesium. On the one hand, the large size of the steel chamber makes a homogeneous heating of the system not only technically challenging but prone to the creation of cold spots, reducing the vapour density at the position of the fibre. With this it takes accordingly longer until the entire fibre is in equilibrium with the background pressure and homogeneously filled. Uneven filling along the fibre length additionally creates severe static electric fields, troublesome for experiments with e.g. Rydberg atoms [12]. In this paper we present a new type of vapour cell that is entirely made out of glass. This includes a new way to mount the fibre inside the cell. These cells are not much larger than the fibre itself and offer an extended stem. Both regions are encapsuled by an appropriate two-zone oven, preventing condensation in the main part by keeping the stem slightly cooler. Moreover, since our design allows full optical access from the side, we can monitor the evolution of the atomic density distribution along the whole fibre length through the measurement of radially emitted fluorescence. From spatially resolved fluorescence we can deduce on what timescale the atoms diffuse into the fibre. Finally we modelled the frequency-dependent absorption of the light propagating inside the hollow-core using a 5-level system to obtain a quantitative understanding of the diffusion process. At first, we present the concept of the gas-cell and how to hold the fibre properly. To study the dynamics of the filling process, we start in an equilibrium situation at a certain temperature and then suddenly raise or drop T and monitor how long it takes to undergo thermalisation.

2. Experimental setup

Optical setup. Our setup is depicted in Fig. 1a. The pump comes from a linearly polarised Toptica DL-pro operated at 780 nm. The pump beam is split into two independent paths, both being sent to the gas-cell. The power of each beam line is controlled by a combination of half waveplate and polarisation beam-splitter cube. We use a second half waveplate to adjust the polarisation state at the entrance of the cell. One beam is coupled to a 60 µm core diameter Kagomé fibre using a lens with 100 mm focal distance. A scanning electron micrograph of the end face of the fibre is shown in Fig. 1b. The fibre is 7.5 cm long. The second beam propagates freely through the gas-cell. At the output of the cell we monitor the transmitted power of the two beams with two photodiodes. Optical bandpass filters are inserted to prevent ambient light from perturbing the detected signal. The glass cell consist of a $\varnothing \times L = 30 \times 80\,\mathrm{mm}^2$ tube made of borosilicate where the optical fibre is placed. To ensure that the fibre is kept straight, we shrunk a 5 mm thick borosilicate tube around the bare optical fibre. The fibre-in-tube is not only more sturdy and can be hold in place with two glass supports, but due to the large thickness we are able to distinguish between fluorescence emitted in the hollow-core fibre and the background outside of it. This background

light stems from leakage out of the fibre, non-perfect coupling and emitted fluorescence. Such a design gives access from the side over the complete length of the fibre, allowing side-scattering measurements. A secondary $\varnothing \times L = 5 \times 45\,\mathrm{mm}^2$ tube is connected at 90° to the main cell and acts as the reservoir. When the cell is sealed before its first use, liquid alkali metal is poured into the reservoir. In the current case we filled our cell with rubidium with its natural isotope distribution. The temperature of the reservoir and of the main cell can be addressed independently. The temperature of the reservoir is kept lower than that of the main cell. Therefore, not only is the atomic density given by the stem temperature but no Rb atoms will stick to the walls of the main cell. The diffusion of the rubidium atoms from the reservoir into the main cell is quite fast given the small dimensions and a steady state is achieved almost instantaneously. To accelerate the diffusion of the atoms into the fibre, we use elevated temperatures, increasing the overall atomic density. In principle we could work up to 300° or even above, but for technical reason we limit us to the range of 45 to 80°.

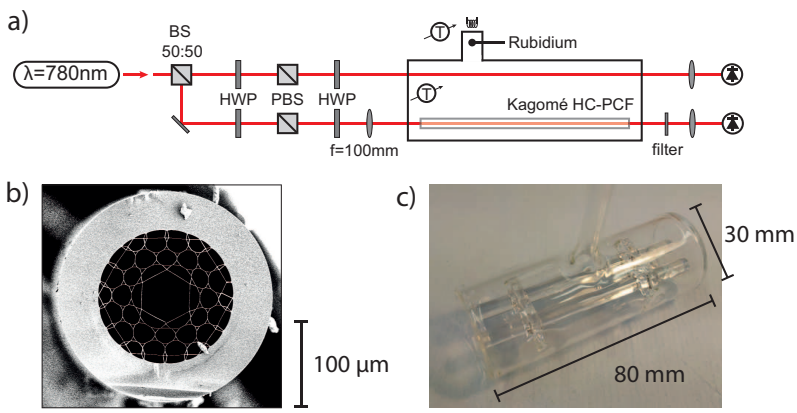

Figure 1. (a) Sketch of the experimental setup. The input beam at 780 nm is initially split equally by a 50:50 beam-splitter BS. Half-wave plates (HWP) and polarisation beam splitter (PBS) ensure the control of the power and a second HWP the input polarisation. One beam is free-space propagating through the cell and the other is coupled into a 60 µm core diameter Kagomé hollow-core PCF shown in **(b)**. At the output of the vapour cell, the beams are separately focused onto photodiodes, with frequency filters in front. **(c)** is the all-glass vapour cell. The temperature of the reservoir and of the main cell can be addressed independently.

Filling the vapour cell and the fibre. Ensuring a constant atomic density inside the fibre is of vital interest for experiments involving, e.g. Rydberg states. In order to monitor the filling process, we constantly measure the spectra after our fibre and of a free-space beam through the glass cell itself, while scanning the probe wavelength through the complete D2 line of rubidium. We target the ^{85}Rb F = 2 line and model it using a Maxwell-Bloch equation approach, including the hyperfine states but neglecting the magnetic sublevels. In order to take into account the small beam size inside our fibre, we include transit time broadening [13] in our 5-level-system (^{85}Rb; F = 2,3; F$'$ = 1,2,3, Figure 2). The evolution of the density matrix is governed by the Lindblad master equation [14]

$$i\hbar\frac{\partial\rho}{\partial t} = [H,\rho] + i\hbar L_D(\rho), \tag{1}$$

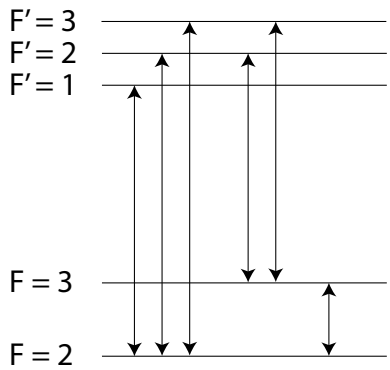

Figure 2. 5-level-system used for the retrieval of the atomic density distribution.

with H the Hamiltonian of the system, ρ the density matrix and $L_D(\rho)$ the Lindblad operator. The measured spectrum corresponds to the steady state solution of equation (1), which yields the excited state fraction of the system. The off-diagonal elements lead to the complex valued electric susceptibility χ and thus the absorption coefficient. To ensure absolute calibration of the frequency-axis, part of the pump beam is guided through a Fabry-Perot interferometer. For intensities below the saturation intensity, we cross-checked our model to the ElecSus open source software [15] for which length, temperature, magnetic field, light polarization, etc. can be adjusted. Note that ElecSus does not take power broadening into account, but it is implemented in our model. In our case, we work above saturation intensity and have to include this in our simulations. Beside the intensity, the temperature of the reservoir is the only fitting parameter, which yields the atomic density via the perfect gas law.

Figure 3 shows the evolution of the atomic density of rubidium in the vapour cell and inside the Kagomé fibre for different temperatures of the cell and of the reservoir. At all times we make sure that the temperature of the reservoir remains lower than that of the main cell. In the initial stage (Figure 3a) the vapour cell is heated from room temperature to 80 °C and left there for 96 h. During that time, the reservoir is left at ambient temperature and only heats up due to the conduction of the oven, reaching 45 °C. As shown in Figure 3a, as the oven is switched on, the density of atoms in the main cell rapidly increases (blue line). Surprisingly, the estimation of the density of rubidium retrieved from the spectrum at the output of the fibre overshoots the value that is expected for such a temperature of the reservoir. We reproducibly observe this whenever we turn on the system. One possible reason being, that even at room temperature rubidium metal diffused into the fibre and stuck to the core wall. When we then increase the temperature, those atoms might desorb and after roughly 5 h the system has relaxed. Afterwards the density inside the fibre increased with a time constant of 45 h. In a second step – after 96 hours – we increased the reservoir temperature to 65 °C, while keeping the cell temperature at 80 °C. As seen in Figure 3b, the average density in the cell (blue line) follows almost instantaneously the set temperature of the reservoir. In case of our Kagomé fibre (green line), we also observe this rapid change, but the atomic density reached an equilibrium after $\sim$24 h, with a timescale of 9.4 h for the diffusion process. This should be compared to the previous experiment using a 60 µm core diameter Kagomé fibre. At that time the

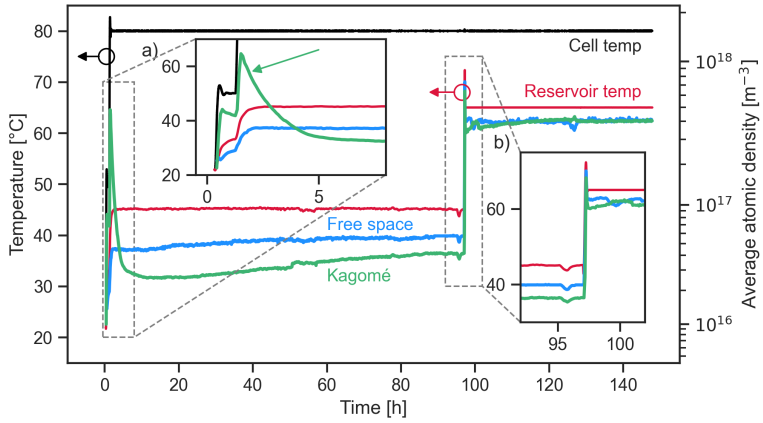

Figure 3. Evolution of the atomic density of rubidium in the vapour cell (blue) and inside the Kagomé fibre (green) vs. the temperature of the cell (black) and of the reservoir (red). The insets magnify the regions where the atomic densities rapidly change due to a modification of the temperatures. The green arrow indicates the apparent overshooting of the density inside the hollow-core when the system is switched on.

filling process lasted >20 days [16].

To even better understand the diffusion in/out of the fibre for an increase/decrease of the gas pressure in the main cell, we additionally look at the radial fluorescence along the fibre. In a simple picture, the atomic density should be proportional to the emitted fluorescence. As a proof of principle, we decrease the temperature of the cell, corresponding to a reduction of the atomic density in the surrounding glass cell and causing a density gradient between the fibre and the cell. We chose a temperature decrease, giving us more time for a careful study of the system dynamics. Specifically, we decreased the reservoir temperature from 65 to 45 °C while keeping the cell temperature at 80 °C and monitored the diffusion process over 100 h. While the rubidium diffuses out of the fibre, we take a series of pictures using a 14-bit CCD camera mounted above our glass cell. To obtain a full spectrum we scan the laser over the the D2 F = 2 transition of ^{85}Rb and image the glass cell every 17.5 MHz of laser detuning. The input polarisation was chosen so that maximum intensity was recorded by the CCD camera. The complete scan takes 25 s, which is well below the diffusion timescale that we measured previously (Figure 3). Each image is transversally integrated within the ROI to obtain a one-dimensional intensity distribution along the propagation. By stacking these 160 pictures for all recorded frequencies, we obtain a two-dimensional map of the emitted fluorescence as a function of detuning and fibre position as shown in Figure 4. The resolution of these maps is around $160 \times 870\,\mathrm{px}^2$ (detuning $\times$ length), depending on the acquisition speed of the camera. On Figure 4b and c the black lines represent the raw experimental data for two specific frequencies and the blue lines our model.

We extract the evolution of the density inside the fibre for a specific detuning Δ of the pump using the Beer-Lambert law. This is done in an iterative way along the whole length of the fibre, assuming an initial intensity $I(z = 0)$ and an atomic density

$\eta(z=0)$. As the light propagates the intensity decreases according to

$$\frac{\mathrm{d}I}{\mathrm{d}z} = \frac{4\pi}{\lambda}\,\mathrm{Im}\left\{\sqrt{1+\chi\left[\eta(z), I(z), \Delta\right]}\right\} I(z) \tag{2}$$

where the susceptibility χ depends on the atomic density $\eta(z)$ and on the light intensity $I(z)$. As we lower the temperature of the reservoir, the density of atoms inside the cell will decrease, yielding a symmetric diffusion of atoms out of both ends of the fibre. For simplicity, we assume that the atomic density distribution follows

$$\eta(z) = (\eta_c - \eta_e)\cdot\left\{1 - \tanh^2\left[\sigma\cdot\left(z - \frac{L}{2}\right)\right]\right\} + \eta_e, \tag{3}$$

with L the fibre length, η_e and η_c respectively the atomic density at both ends and at the center of the fibre. σ is chosen so that $\eta(0) = \eta(L)$ is within 1% of η_e. This approximately corresponds to a factor of $\sigma = \frac{6}{L}$. The measured fluorescence (black

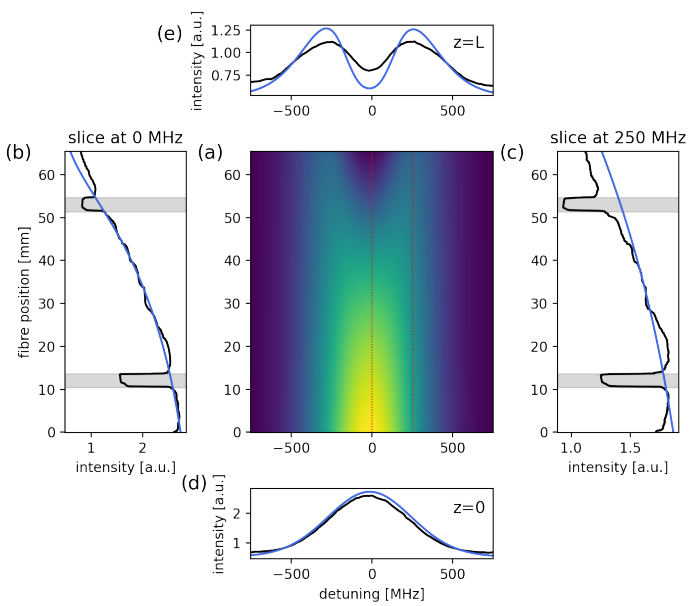

Figure 4. (a) Two-dimensional map of fluorescence emitted by rubidium atoms inside a HC-PCF as a function of detuning and fibre position at 65 °C. Light is entering the cell from the position '0'. Black indicates experimental data and blue the best fit. The grey area marks the position of the fibre holders, which were ignored for fitting. **(b)** and **(c)** illustrate the fluorescence along z along at respectively 0 and 250 MHz indicated by the dotted lines. **(d)** and **(e)** show the spectrum at the beginning ($z=0$) and end ($z=L$) of the fibre.

lines in Figure 4b, c is directly linked with the atomic density and the excited state fraction. Combining the steady state solution of (1) with the assumed distribution of (3), we calculate η_e and η_c. As shown on Figure 4b and c the calculated fluorescence curves (blue lines) along the fibre length agree very well with our experimental data. Figure 4d and e show the fluorescence spectra at the beginning and the end of the fibre at a given time t. As the diffusion process takes place, we record a series of these

maps which are processed the same way. Figure 5a shows the temporal evolution of the atomic density at the end (η_e) and in the center (η_c) of the fibre. It is clear that the atomic density at the edge rapidly decreases (green curve) following the change in the cell. The change in the center (blue curve) is much slower, because the rubidium atoms need to diffuse out of the fibre. Like the transmission measurement (Figure 3a), the fluorescence measurement shows that the atomic density rapidly changes as soon as the reservoir temperature is modified (Figure 5a). After this abrupt drop the evolution of the atomic density is much slower, with timescales of $\tau_c = 36\,\mathrm{h}$ and $\tau_e = 45\,\mathrm{h}$, when fitting with a double exponential decay of the form

$$\eta(t) = ae^{-t/\tau_1} + be^{-t/\tau_2} + c. \tag{4}$$

Here τ_c respectively τ_e is the larger of the two lifetimes τ_1/τ_2, corresponding to the slower diffusion timescale of the system.

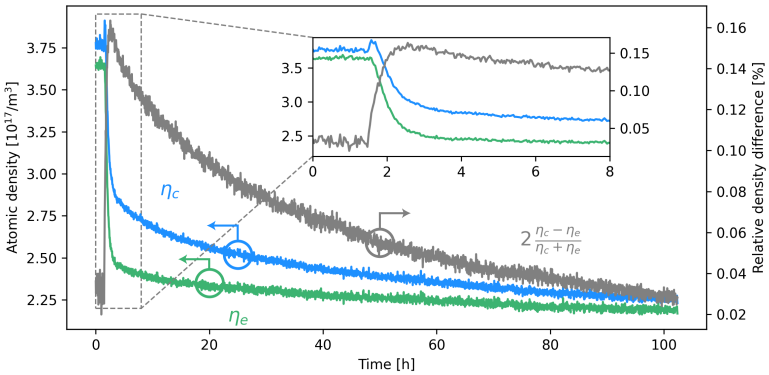

Figure 5. Retrieved atomic densities at the center (blue) and edges (green) of a 60 µm Kagomé fibre when decreasing the reservoir temperature from 65 to 45 °C while keeping a constant cell temperature of 80 °C. The grey curve is the relative density change $2\,(\eta_c-\eta_e)/(\eta_c+\eta_e)$.

To conclude, we presented here an all-glass assembly integrating alkali vapours with a hollow-core photonic crystal fibre. Its small dimensions and homogeneous temperature permit a rapid modification of the atomic density in a controlled way. Additionally, the all-glass design allows to perform easily accessible measurements from the side. Measuring the fluorescence of the rubidium allows observing in real-time and spatially resolved the diffusion of the atoms out of the fibre when changing the atomic density inside the vapour cell. Both transmission and fluorescence measurements confirm that the atomic density inside the fibre has reached an equilibrium only after a few days. This drastically contrasts with previous experiments, where hollow-core fibres were filled with hot alkali metal in bulky metal based vacuum chambers [12]. We believe that such a cell makes an attractive tool for atomic spectroscopy, Rydberg physics and non-linear optics. Its small size makes this type of cells more transportable and integration in an spectroscopy setup much easier. In a next step it would be interesting to have an all fibre based setup to avoid free beam coupling to the fibre [17].

Acknowledgements

This project is supported by the DFG (JO 1090/4-1, LO 1657/6-1 & RU 1426/1-1) as part of the SPP 1929 "Giant Interactions in Rydberg Systems (GiRyd)". We also thank SAOT for financial support.

3. References

[1] Ioannis Caltzidis et al. 'Atomic Faraday beam splitter for light generated from pump-degenerate four-wave mixing in a hollow-core photonic crystal fiber'. In: Physical Review A 103.4 (2021). Publisher: American Physical Society, p. 043501.

[2] C. F. McCormick et al. 'Strong relative intensity squeezing by four-wave mixing in rubidium vapor'. In: Optics Letters 32.2 (2007). Publisher: Optical Society of America, pp. 178–180.

[3] Ran Finkelstein et al. 'Fast, noise-free memory for photon synchronization at room temperature'. In: Science Advances (2018). Publisher: American Association for the Advancement of Science.

[4] K. T. Kaczmarek et al. 'High-speed noise-free optical quantum memory'. In: Physical Review A 97.4 (2018). Publisher: American Physical Society, p. 042316.

[5] Dmitry Budker and Michael Romalis. 'Optical magnetometry'. In: Nature Physics 3.4 (2007). Bandiera_abtest: a Cg_type: Nature Research Journals Number: 4 Primary_atype: Reviews Publisher: Nature Publishing Group, pp. 227–234.

[6] David H. Meyer, Paul D. Kunz and Kevin C. Cox. 'Waveguide-Coupled Rydberg Spectrum Analyzer from 0 to 20 GHz'. In: Physical Review Applied 15.1 (2021). Publisher: American Physical Society, p. 014053.

[7] John C. Travers et al. 'Ultrafast nonlinear optics in gas-filled hollow-core photonic crystal fibers [Invited]'. In: JOSA B 28.12 (2011). Publisher: Optical Society of America, A11–A26.

[8] Ana M. Cubillas et al. 'Photonic crystal fibres for chemical sensing and photochemistry'. In: Chemical Society Reviews 42.22 (2013). Publisher: The Royal Society of Chemistry, pp. 8629–8648.

[9] G. Epple et al. 'Rydberg atoms in hollow-core photonic crystal fibres'. In: Nature Communications 5.1 (2014). Number: 1 Publisher: Nature Publishing Group, pp. 1–5.

[10] Saikat Ghosh et al. 'Low-Light-Level Optical Interactions with Rubidium Vapor in a Photonic Band-Gap Fiber'. In: Physical Review Letters 97.2 (2006). Publisher: American Physical Society, p. 023603.

[11] P. S. Light et al. 'Electromagnetically induced transparency in Rb-filled coated hollow-core photonic crystal fiber'. In: Optics Letters 32.10 (2007). Publisher: Optical Society of America, pp. 1323–1325.

[12] G. Epple et al. 'Effect of stray fields on Rydberg states in hollow-core PCF probed by higher-order modes'. In: Optics Letters 42.17 (2017). Publisher: Optical Society of America, pp. 3271–3274.

[13] A Urvoy et al. 'Optical coherences and wavelength mismatch in ladder systems'. In: Journal of Physics B: Atomic, Molecular and Optical Physics 46.24 (2013), p. 245001.

[14] Daniel Adam Steck. Quantum and Atom Optics. Google-Books-ID: bc9TMwEACAAJ. 2007. 835 pp.

[15] Mark A. Zentile et al. 'ElecSus: A program to calculate the electric susceptibility of an atomic ensemble'. In: Computer Physics Communications 189 (2015), pp. 162–174.

[16] Georg Epple. 'Spectroscopy of Rydberg Atoms in Hollow-Core Photonic Crystal Fibers'. PhD thesis. 2017.

[17] Josephine Gutekunst et al. 'Fiber-integrated spectroscopy device for hot alkali vapor'. In: Applied Optics 56.21 (2017), p. 5898.